Acta Crystallographica Section D
Biological Crystallography
ISSN 0907-4449

Quantitative imaging by confocal scanning fluorescence microscopy of protein crystallization *via* liquid–liquid phase separation

Denis Vivarès, Eric W. Kaler and Abraham M. Lenhoff*

Center for Molecular and Engineering Thermodynamics, Department of Chemical Engineering, University of Delaware, Newark, DE 19716, USA

Correspondence e-mail: lenhoff@che.udel.edu

Received 16 July 2004
Accepted 12 November 2004

Metastable states such as liquid–liquid phase separation, aggregation and gelation can affect protein crystallization but their positive or negative effects are only partially understood. In this work, mixtures of PEG (MW 10 kDa) and a large model protein, glucose isomerase (MW 173 kDa), have been studied to characterize the effect of a metastable liquid–liquid phase separation on protein crystallization. Fluorescence labeling allowed confocal fluorescence microscopy observations and quantification of the partitioning of the protein and PEG between the liquid phases and showed two steps in the crystallization process. Two crystallization mechanisms within the liquid domain were revealed, yielding two different polymorphs. With one polymorph, few crystals nucleated and grew droplet-by-droplet in the dispersed concentrated liquid phase, while for the other homogeneous crystal nucleation and growth occurred independently and simultaneously in numerous droplets of the concentrated phase. The results demonstrate the substantial possible complexity of crystallization behavior, as well as its sensitivity to the location of the conditions on the phase diagram and to the physicochemical properties of the system.

1. Introduction

Commonly used crystallizing agents [*e.g.* salt, polyethylene glycol (PEG)] and physicochemical parameters (*e.g.* temperature, pressure, pH) can lead not only to the desired solid (crystal)–liquid phase separation but also to several other metastable phase separations, of which liquid–liquid phase separation, aggregation and gelation are the most common. These kinds of phase behavior can accelerate, retard and even stop the nucleation and growth of protein crystals. Liquid–liquid phase separation (LLPS) has been the metastable phase separation most widely studied to date. Microscopy observations of the nucleation and growth of protein crystals *via* a LLPS have been reported by several groups, usually in the presence of PEG (Alber *et al.*, 1981; Collier *et al.*, 1982; Ray & Bracker, 1986; Kuciel *et al.*, 1992; Harris *et al.*, 1995; Kuznetsov *et al.*, 2001; Chen *et al.*, 2004). In these cases, Ray and Bracker proved that crystals usually nucleate at the surface of the liquid droplets and Kuznetsov *et al.* noted that the crystals appeared to grow from the phase boundary exclusively into the protein-lean phase. These phenomena are not limited to soluble proteins, and indeed, in many mixtures of membrane protein, PEG, and detergent crystallization occurs *via* a LLPS, with the protein-detergent complexes partitioning and crystallizing inside or at the surface of detergent-rich droplets (Michel, 1991).

All the above observations were essentially qualitative, and quantitative insights have come primarily from numerical simulations and thermodynamic models, which predict that the nucleation of protein crystals should be enhanced close to the critical point (ten Wolde & Frenkel, 1997) or *via* a LLPS (Haas & Drenth, 1998). In both cases, the first step in the process is thought to be the creation of a protein-rich droplet inside which nuclei are subsequently formed. Haas and Drenth (Haas & Drenth, 2000) have also suggested that crystal growth should be favored if the growing crystal is surrounded by a protein-rich layer. These theoretical predictions were partly corroborated by experimental studies (Muschol & Rosenberger, 1997; Galkin & Vekilov, 2000), which have shown that the nucleation rate was enhanced and the nucleation time reduced in samples with compositions around the liquid–liquid phase boundary.

Here we augment these previous investigations with an *in situ* time-lapse quantitative study that shows the nucleation and growth of protein crystals during a metastable liquid–liquid phase separation. We focused our studies on PEG/soluble protein mixtures. Many recent reports (Budayova *et al.*, 1999; Kulkarni & Zukoski, 2001; Annunziata *et al.*, 2002; Tanaka & Ataka, 2002; Vivarès & Bonneté, 2002; Annunziata *et al.*, 2003; Tanaka *et al.*, 2003; Tessier *et al.*, 2003; Vivarès & Bonneté, 2004) have shown that the attractive protein–protein interactions induced by the addition of PEG, usually referred to as depletion interactions, favor liquid–liquid and/or liquid–solid phase separations in protein solutions. In an ideal case, and for a given polymer size and concentration, the depletion attraction increases with the protein size (Asakura & Oosawa, 1958; Vrij, 1976). We therefore chose to work with glucose isomerase from *Streptomyces rubiginosus*, which is a large, commercially available protein (MW 173 kDa). We present here the results obtained with a PEG of 10 kDa molecular weight. The principal experimental tool is confocal scanning laser microscopy (CSLM), which has been extensively used in recent years to study phase separation involving colloids, *e.g.* de Hoog *et al.* (2001), or biopolymers, *e.g.* van de Velde *et al.* (2003). We have taken advantage of this technique to investigate the two-step crystallization mechanism inside the metastable liquid–liquid demixing zone using labeled protein and polymer. Quantitative CSLM experiments were performed to determine the PEG and protein compositions of both phases. Two different polymorphs were characterized and, depending upon the polymorph, two very different crystal growth mechanisms were characterized. Furthermore, the monitoring of the protein concentration by CSLM during crystallization enabled explanation of the final properties of the crystallized solutions.

2. Materials and methods

2.1. Preparation of protein, PEG and salt solutions

Glucose isomerase from *Streptomyces rubiginosus* was purchased from Hampton Research as a crystalline suspension in an ammonium sulfate-rich solution. The protein is particularly stable between pH 6 and pH 8 but begins to denature below pH 5 (http://www.hamptonresearch.com/support/guides/7100G.pdf). Studies were therefore made in either a 10 m*M* Tris buffer pH 7, or in a 10 m*M* MES buffer, pH 6.5. The crystalline suspension was dialyzed extensively at room temperature in a 10 ml Slide-A-Lyzer® cassette (from Pierce) against the 10 m*M* Tris pH 7 buffer. The crystals dissolve quickly in the first few hours of the dialysis. The resulting protein solution was then concentrated to the desired final concentration using a 10k MWCO Amicon Ultra-4 centrifuge and filter device (from Millipore). The protein concentration was determined by measuring the UV absorbance at 280 nm using an extinction coefficient of $1.0\ \mathrm{cm^2\ mg^{-1}}$ (http://www.hamptonresearch.com/support/guides/7100G.pdf). The final protein solution was dialyzed against a 10 m*M* MES pH 6.5 buffer for studies at pH 6.5.

PEG 10 kDa was purchased as a powder from Fluka. 40%(*w*/*v*) stock solutions were obtained by dissolution of the appropriate amount of polymer with the 10 m*M* Tris pH 7 or the 10 m*M* MES pH 6.5 buffer solutions. Sodium chloride (from Sigma-Aldrich) was dissolved in the appropriate buffer solution to obtain a final concentration of 5 *M*.

All the buffer, protein and salt solutions were filtered through 0.22 µm Millipore sterile filters. The 40% PEG 10 kDa solutions were filtered through a 0.8 µm Millipore sterile filter.

2.2. Phase diagram determination

The phase diagram determination and microscopy experiments were carried out in a 10 m*M* pH 7 buffer at room temperature ($T = 24 \pm 2$°C). Without any salt addition and starting with PEG concentrations between 0 and 20% and protein concentrations between 0 and 50 mg ml^{-1}, no liquid–liquid phase separation was observed, probably because these conditions are such that the proteins are charged. All other experiments were carried out with identical fairly high salt concentrations of 0.5 *M* NaCl to screen the electrostatic interactions. The solubility curve was determined by seeding the PEG/protein mixtures with crushed microcrystals at different PEG concentrations. The protein concentration in the supernatant was followed for several weeks by UV spectroscopy and the protein solubility taken as the final stable protein concentration.

The liquid–liquid phase boundary, or cloud point curve, and the aggregation curve were characterized by preparing different mixtures of protein and PEG. Small equal volumes (a few microliters) of concentrated protein solution and PEG solution were mixed, put under a layer of paraffin oil in Microbatch plates (both from Hampton Research) and observed by optical microscopy to detect any phase separation.

2.3. Confocal scanning laser microscopy experiments

Confocal scanning laser fluorescence microscopy experiments were performed using an inverted Zeiss LSM 510 microscope under 20× Plan-Apochromat and 40× (under oil immersion) Plan Neo-Fluar objectives.

2.3.1. Labeling reactions. PEG cannot be directly labeled, so PEG-NH_2 10 kDa (Nektar Therapeutics) was used for the labeling procedure (Sukhishvili *et al.*, 2002). PEG-NH_2 10 kDa was labeled with fluorescein isothiocyanate (FITC) (Sigma–Aldrich) or Cy5 (a cyanine derivative dye) (Amersham Biosciences) while the glucose isomerase was labeled with Cy5. For labeling, 100 mg of PEG-NH_2 was dissolved in 500 µl of 100 m*M* sodium carbonate pH 9. This solution was then either poured directly into a vial containing 10 mg of Cy5 crystals or mixed with a 500 µl ethanol solution containing 10 mg of FITC. To label the protein with Cy5, a solution containing about 20 mg of glucose isomerase was dialyzed against 100 m*M* sodium carbonate, pH 9, and directly poured into the kit vial containing 10 mg of Cy5 crystals. All the solutions were then gently stirred overnight. The labeled products were separated from the unreacted dyes using a Sephadex G-25 size exclusion column running with the 10 m*M* Tris pH 7 buffer. The final labeled polymer and protein solutions were concentrated using respectively a 5k or 10k MWCO Amicon Ultra-4 centrifuge and filter device to approximate final concentrations of 5%(*w*/*v*) for the polymer solution and 20 mg ml^{-1} for the protein solution. These final labeled solutions were dialyzed against the 10 m*M* MES pH 6.5 buffer solution to perform the studies at pH 6.5. For the microscopy observations, typically 1.5 µl of the 20 mg ml^{-1} labeled protein solution was mixed with 80 µl of a 240 mg ml^{-1} unlabeled protein solution and 100 µl of the 5% labeled PEG-NH_2 solution mixed with 900 µl of a 40% unlabeled PEG solution. The amount of labeled PEG-NH_2 or protein introduced in the unlabeled PEG or protein solutions was therefore always negligible. From these stock solutions, 2 µl of a protein solution and 2 µl of a polymer solution of desired concentrations were then mixed vigorously and placed in a 35 mm glass bottom microwell dish (Mattek Corporation) under a 2 ml layer of paraffin oil to prevent any evaporation during the experiments.

2.3.2. Qualitative and quantitative analysis. A qualitative characterization of the redistribution of the polymer and the protein into

the two liquid phases was obtained by simultaneously exciting FITC and Cy5 with the 30 mW ArKr (λ = 488 nm) and the 5 mW HeNe (λ = 633 nm) laser sources respectively. The emitted fluorescence intensities also allow, in principle, the quantitative determination of the concentrations of the two components, but doing this directly in the two-color mixtures was complicated by non-negligible energy transfer between FITC and Cy5 and by some non-linearity in the fluorescence intensity dependence on the polymer concentration. We therefore performed the quantitative analysis separately with either the protein or the polymer labeled with Cy5. Note that both the cloud point measurements and the crystallization mechanisms were identical with or without labeled components. The laser powers were low enough to avoid any photodegradation of the dyes, which could lead to a continuous decrease of the fluorescence intensity with time. *Z*-stack sections of *xy* horizontal planes were acquired for distances between 0 and 20 µm from the cover-slide. The resulting stable fluorescence values averaged within a single phase over the *xy* plane were recorded. The overall label ratio, controlled by the proportions in which labeled and unlabeled solutions were mixed, was adjusted in order to minimize the scattering of fluorescence by the coverslide. Finally, the residual intensity from the buffer was subtracted before analysis. To determine the calibration curves in the protein and polymer concentration ranges of interest, different solutions ranging in concentration from 0 to 14% for the polymer and 0 and 230 mg ml^{-1} for the protein were prepared. As we could not concentrate the protein solution to a concentration higher than approximately 250 mg ml^{-1}, the reference point for the highest intensity for the protein calibration curve, which was needed to probe the protein concentration in the dense phase accurately, was taken as the protein concentration in the crystal, *i.e.* about 600 mg ml^{-1} for the *I*222 space group. The main uncertainties came from the broad spectrum of the fluorescence intensity emitted by the crystals, but the calibration curves were linear if the average value of the crystal fluorescence was used.

2.4. Characterization of the two polymorphs

To determine if the two crystal forms grown at either pH 7 or pH 6.5 were the same polymorph or two different polymorphs, we performed simple crystal growth experiments. Crystals of the two forms were picked directly from the final solutions of demixing/crystallization experiments and placed in a solution of 4% PEG 10 kDa, 50 mg ml^{-1} glucose isomerase, 500 m*M* NaCl, 10 m*M* Tris pH 7. In this solution, the crystal form grown at pH 7 continues to grow whereas the other crystal form, grown at pH 6.5, dissolves. Identical observations were made in several other solutions. These experiments prove unambiguously that these two crystal forms are different polymorphs.

3. Results

3.1. Glucose isomerase – PEG 10 kDa phase diagram

Fig. 1 shows the experimental glucose isomerase/PEG 10 kDa phase diagram at pH 7 for protein concentrations between 0 and 200 mg ml^{-1} and polymer concentrations between 0 and 14%. The phase diagram contains three distinct curves, namely the solubility curve at lower protein and PEG concentrations and the LLPS curve (or cloud point curve) and the aggregation curve at higher concentrations. Beyond the liquid–liquid phase boundary, the mixture becomes cloudy and discrete droplets 10 to 100 µm in diameter are visible under an optical microscope. This process is reversible and the sample clears upon dilution. When samples are held above the LLPS curve, after a few minutes to a few days only crystals in equilibrium with a single liquid phase are present, which proves the metastability of the LLPS. The aggregates, at least close to the aggregation curve, become crystalline within one hour, which also proves their metastability. In the next sections, we discuss only the crystallization mediated by the LLPS, *i.e.* all studies were done in the demixing zone between the cloud point and the aggregation curve.

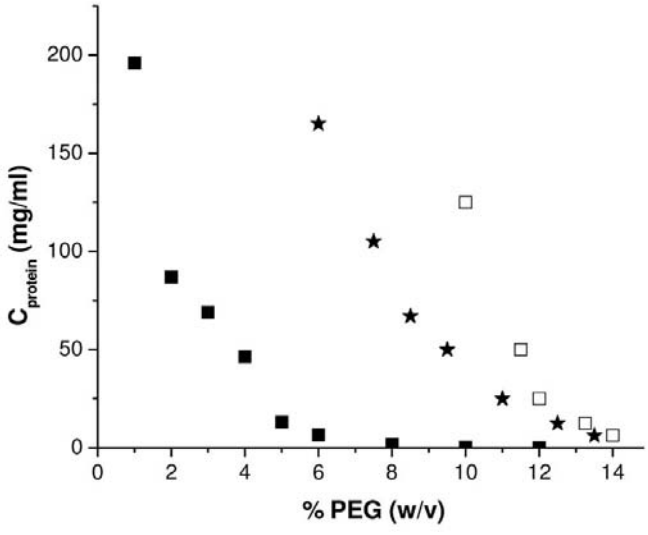

Figure 1
The glucose isomerase/PEG 10 kDa phase diagram (0.5 *M* NaCl, 10 m*M* Tris pH 7) containing the solubility curve (filled squares), the LLPS or cloud point curve (stars) and the aggregation curve (open squares).

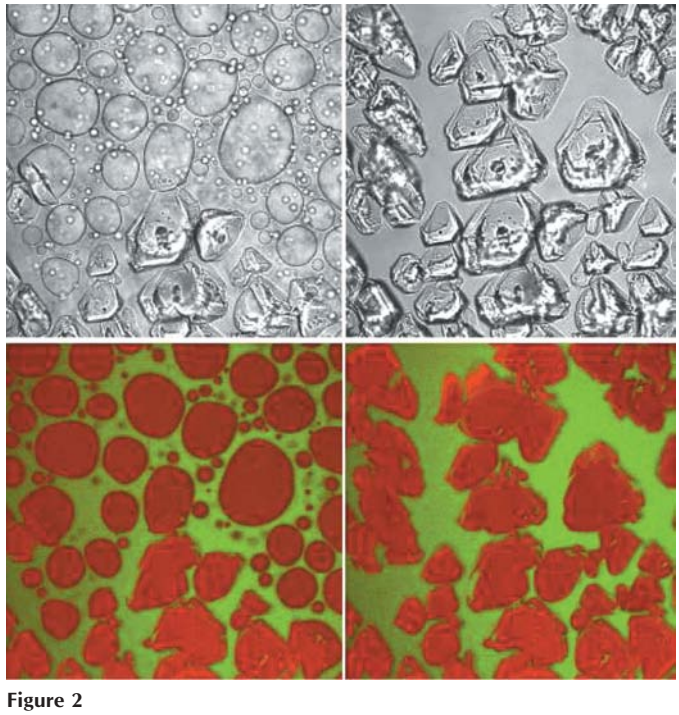

Figure 2
CSLM bright field (top) and fluorescence (bottom) images of the 'droplet-by-droplet' mechanism. The protein is labeled with Cy5 (red) and the polymer with FITC (green). The first picture on the left was taken within 30 min after mixing, and the time interval between the two pictures was 380 s. ($C_{protein}$ = 55 mg ml^{-1}, $C_{PEG10\,kDa}$ = 9.5%, 0.5 *M* NaCl, 10 m*M* Tris pH 7; dimensions of each picture: 326 µm × 326 µm). Colour versions of the figures in this article are available in the online edition of the journal.

3.2. Qualitative CSLM observations

The results of a typical time-lapse CSLM experiment in the metastable demixing zone are shown in Fig. 2. The two-laser setup enabled imaging separately and simultaneously the fluorescence signals emitted by the Cy5-labeled protein (in red) and by the FITC-labeled polymer (in green) as well as the classical transmitted optical light. The protein partitions predominantly in the dense droplets, which coalesce and settle with time, whereas the polymer is found mainly outside the droplets. Depending upon the initial conditions, a few crystals (usually fewer than five in a 4 µl volume) with a dendritic shape appear in the field of view within 0 to 30 min (not shown in the pictures). It was not possible to distinguish in which phase (outside or inside the droplets) these first crystals nucleate. After having settled at the bottom of the sample, these first crystals grow by a 'droplet-by-droplet' mechanism: as soon as a crystal touches the surface of a protein-rich droplet, the crystal growth keeps going inside the droplet, which eventually becomes entirely crystalline in only a few minutes. Once the crystal (or any part of it) is no longer in contact with the dense droplet, its growth is almost completely arrested. The final structure of the solution is therefore similar to the initial one, but with the droplets replaced at exactly the same positions by crystalline material. The crystals are not perfectly faceted. In some cases when the crystallization was sufficiently delayed to allow the formation of a continuous dense layer due to droplet settling and coalescence, crystal growth occurred inside this layer, which eventually transformed itself completely into a single crystal.

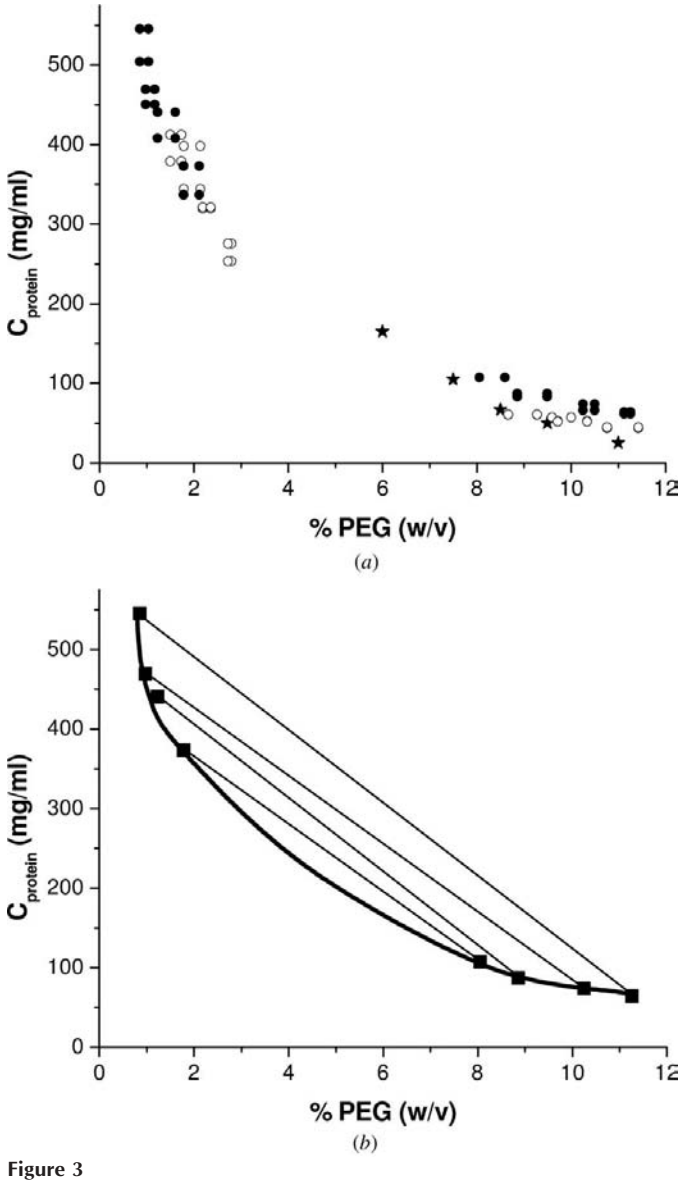

Figure 3
(*a*) Comparison between the cloud point measurements (stars) and the CSLM analysis for two different initial protein concentrations, $C_{protein}$ = 55 mg ml^{-1} (open circles) and $C_{protein}$ = 125 mg ml^{-1} (filled circles). (*b*) The tie-lines resulting from a coupled CSLM experiment with an initial protein concentration of 125 mg ml^{-1}; the phase boundary is drawn to guide the eye (0.5 *M* NaCl, 10 m*M* Tris pH 7).

3.3. Quantitative CSLM experiments

The classical method to determine the compositions of two equilibrium liquid phases is to separate the phases (*e.g.* by centrifugation) and then analyze their compositions. Typically, the protein and the PEG concentrations can be evaluated by UV-visible spectroscopy and refractometry, respectively (Annunziata *et al.*, 2002). In our case, such a procedure was not possible for two main reasons: (1) the short time in which crystallization occurs and (2) the heterogeneous nucleation induced by centrifugation in many cases. A method for *in situ* characterization of the protein and polymer concentrations was therefore needed, and this can also provide more information than an *ex situ* analysis. *In situ* evaluations of the protein concentration during crystal growth experiments have been performed previously by UV-visible spectroscopy (Kam & Feher, 1978), interferometry (Komatsu *et al.*, 1993) and Raman spectroscopy (Schwartz & Berglund, 1999). On the other hand, quantitative analysis by CSLM of the concentrations in two-phase biopolymer mixtures has been discussed (Blonk *et al.*, 1995; Nordmark & Ziegler, 2000). Following the same idea, we used CSLM to quantify *in situ* and in real time not only the protein concentration but also the polymer concentration during phase separation and crystallization. Concentrations were determined using calibration curves.

Fig. 3(*a*) gives the results obtained from microbatch trials and from several independent CSLM experiments. Two different initial protein concentrations were studied, 55 mg ml^{-1} and 125 mg ml^{-1}, with the corresponding initial polymer concentrations varied from 9.5% to 11% and from 7.5% to 9%, respectively. The lower ends of the polymer concentration ranges were limited by the liquid–liquid phase boundary and the upper ones by the aggregation curve. There is reasonable agreement between the cloud points determined by microbatch experiments and the analysis from the CSLM experiments, demonstrating the validity of the quantitative microscopy. The small discrepancies can be attributed mainly to either (i) the error in the highest protein concentration reference, *i.e.*, the protein concentration in the crystal or (ii) the possibility that equilibrium between the two liquid phases was not always reached in the CSLM experiments. Indeed, because of the rapidity of the crystallization step, which can substantially change the protein concentration in the solution (see below), the quantitative analysis was carried out in the first few minutes after vigorous mixing. For the sake of clarity, Fig. 3(*b*) presents results of only one set of CSLM experiments ($C_{protein\ initial}$ = 125 mg ml^{-1}, four polymer concentrations) including the tie-lines, which highlight the protein and polymer compositions in the respective pairs of equilibrium phases.

Regardless of the initial protein (55 mg ml^{-1} or 125 mg ml^{-1}) or polymer (from 7.5% to 11%) concentrations, the protein concentration in the dense phase is always above 200 mg ml^{-1} and the polymer concentration always below 3%. Note that much higher protein concentrations can be produced *via* a PEG-induced phase separation than by simply centrifuging the samples. In contrast, in the

less dense phase (outside the droplets), the protein and the polymer concentrations are not very far from the initial ones, meaning that this phase is dilute in protein and rich in polymer. This observation reflects the low phase ratio between the dense and light phases, so that it is only because of settling and coalescence of the dense phase that the micrographs, taken at the bottom of the samples, appear to show higher ratios, *e.g.* in Fig. 2.

Analysis of the confocal fluorescence experiments enables not only quantification of the protein and the polymer concentrations initially following the liquid–liquid phase separation, but also those later in the process when crystallization occurs inside the droplets (Fig. 4). Inside a protein-rich droplet, the protein concentration remains very high and hardly changes as the crystal grows. In contrast, as soon as the crystal (or any part of it) is no longer in contact with the dense-phase droplet, the protein concentration locally decreases, creating a depletion zone around the crystal, which grows further only to a very limited extent. Similar experiments showed that the polymer concentrations outside and inside the droplets remains almost constant during the whole demixing-crystallization process (data not shown).

For initial conditions close enough to the liquid–liquid boundary (at the polymer-rich end of the tie-line), the volume of the dense phase is much smaller. As a result, a growing dendritic like crystal depletes all the protein in its dense-phase droplet and starts growing outside the droplet. This creates a depletion zone around the growing crystal and results in the disappearance of the droplets in the vicinity of the growing crystal. In some cases, for conditions essentially on the liquid–liquid phase boundary, the dendritic crystals grow only outside the droplets (data not shown). Slightly further from the phase boundary, however, the growing crystals may touch some droplets that had not totally disappeared, and crystallization by the 'droplet-by-droplet' mechanism follows (Fig. 5).

4.1. An alternative demixing/crystallization mechanism yields a different polymorph

At pH 6.5 (10 m*M* MES), an entirely different mechanism was observed, suggesting the appearance of another polymorph (see details in Materials and methods section). As can be seen in Fig. 6, a very different and more faceted crystal shape is observed. As with the other polymorph, the protein partitions into the dense phase and the polymer into the light phase, and crystallization again occurs in the protein-rich phase. However, the 'droplet-by-droplet' mechanism is not observed, and instead numerous crystals grow independently of each other inside the droplets. Furthermore, nucleation clearly occurs inside the dense droplets. Eventually, as with the other crystal form, as soon as the crystal is no longer wetted by a protein-rich liquid layer, the protein concentration drops in its vicinity and the crystal growth becomes much slower (data not shown). It is noteworthy that in some trials at pH 6.5, both polymorphs nucleated and the two different crystallization mechanisms occurred simultaneously in the same sample.

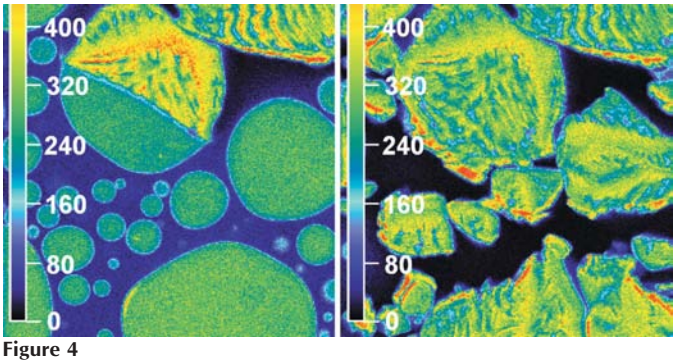

Figure 4
Evolution of the protein concentration during crystallization *via* the 'droplet-by-droplet' mechanism, as characterized by CSLM. The scale on the left of each picture indicates the protein concentration in mg ml^{-1}. The first picture on the left was taken within 30 min after mixing, and the time interval between the two pictures was 225 s. ($C_{\rm protein}$ = 55 mg ml^{-1}, $C_{\rm PEG10\,kDa}$ = 9.5%, 0.5 *M* NaCl, 10 m*M* Tris pH 7; dimensions of each picture: 230 µm × 230 µm).

5. Discussion

The liquid–liquid and crystallization phase behavior observed is governed primarily by the equilibrium phase diagram, but it is also affected by several other physicochemical mechanisms and associated parameters. As regards the phase diagram, the solubility of glucose isomerase decreases with increasing PEG concentration, which is consistent with the pioneering work on several PEG/protein systems of Atha and Ingham (Atha & Ingham, 1981). Furthermore, the liquid–liquid phase separation was found to be metastable towards the solid-liquid phase separation over the whole protein and polymer concentration range investigated, which also appears to be general to PEG/protein systems (Tanaka & Ataka, 2002; Tanaka *et al.*, 2003; Vivarès & Bonneté, 2004). Finally, as revealed by quantitative confocal scanning laser microscopy (CSLM) experiments, the protein concentration in the dense phase was found to be very high, and close to the protein concentration in the crystal, which is also in agreement with previous studies (Ray & Bracker, 1986; Vivarès & Bonneté, 2004). Consequently, in many ways, these results are not specific to the glucose isomerase/PEG 10 kDa system. In the dilute phase, the protein concentration and the polymer concentration were close to

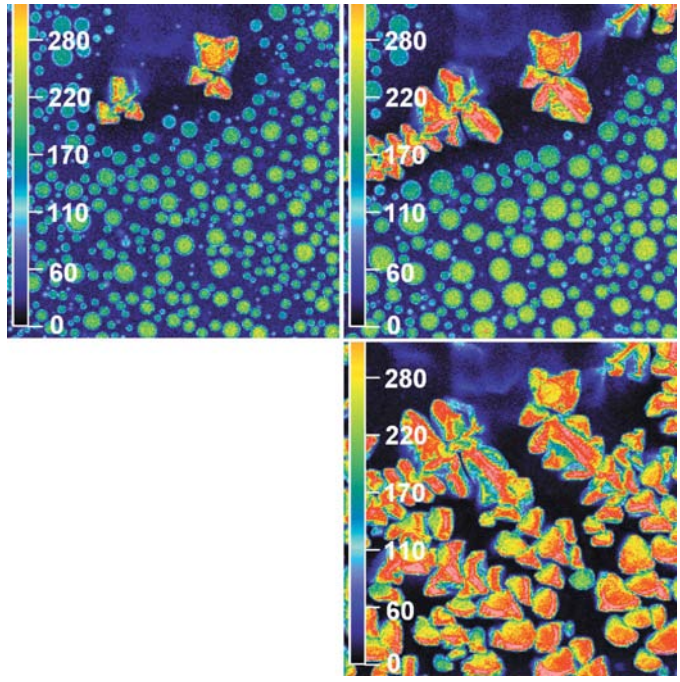

Figure 5
Evolution of the protein concentration characterized by CSLM during an experiment in which the growth mechanism started with crystallization outside the droplets and finished with the 'droplet-by-droplet' mechanism. The scale on the left of each picture indicates the protein concentration in mg ml^{-1}. The first picture (top left) was taken within 30 min after mixing and the time intervals between the first and the last two pictures were 450 s and 880 s, repectively. ($C_{\rm protein}$ = 25 mg ml^{-1}, $C_{\rm PEG10\,kDa}$ = 11.5%, 0.5 *M* NaCl, 10 m*M* Tris pH 7; dimensions of each picture: 326 µm × 326 µm).

the initial ones, which is expected since all of the measurements were carried out close to the dilute part of the liquid–liquid boundary. The resulting phase ratios then play an important role in determining the pattern of behavior observed.

Within the demixing zone, regardless of which polymorph appears, crystal growth occurs inside the protein-rich droplets except close to the liquid–liquid boundary. These observations are consistent with observations of colloids (Faers & Luckham, 1997; Hachisu, 1998) or organic molecules (Bonnett *et al.*, 2003) and with the theoretical predictions of Haas and Drenth (Haas & Drenth, 2000). They suggested that, in the protein-rich phase, protein molecules are always available at the crystal surface, and diffusional limitations are negligible, making the crystal growth step easier, thus crystal growth is favored. The nucleation step could only be imaged in these experiments for the second polymorph, grown at pH 6.5. For this polymorph, multiple independent crystals were observed inside the droplets. This suggests that nucleation takes place inside the droplets *via* a homogeneous mechanism. Homogeneous nucleation followed by crystal growth inside the protein-rich droplets is also consistent with theories (ten Wolde & Frenkel, 1997; Haas & Drenth, 1998). One possible explanation is that the wetting of the nuclei (and then crystals) in the protein-rich phase decreases their interfacial free energy in the solution.

These experimental results showing the nucleation and the growth of protein crystals mediated by an LLPS are very different from those seen previously. In the other PEG/protein mixtures studied, the crystals were reported to nucleate at the surface of the protein-rich droplets and to grow outward into the protein-lean phase (Ray & Bracker, 1986; Kuznetsov *et al.*, 2001). The stark difference in these results could possibly be due to differences in the way the experiments were performed. In previous work, the LLPS was initiated by mixing concentrated salt solutions with dilute polymer solutions. As a result, unlike in our experiments, the protein-rich droplets were also polymer-rich and therefore highly viscous. This viscous medium could suppress both nucleation and growth inside the protein dense droplets (Vekilov, 2004).

The crystal growth at pH 7 occurs *via* the 'droplet-by-droplet' mechanism: as soon as part of the crystal touches a protein-rich droplet, it continues growing inside this droplet. The 'droplet-by-droplet' mechanism always starts with a few dendritic crystals, which first grow outside the droplets, where the supersaturation is very high ($\sigma = C/C_e \simeq 70$ for the initial conditions $C_{\rm protein} = 55$ mg ml^{-1}, $C_{\rm PEG10\,kDa} = 9.5\%$, C being the protein concentration outside the droplets and C_e the protein solubility). Close to but below the liquid–liquid phase boundary in the single-phase region, we could also observe such dendritic crystals. A dendritic crystal is typically observed at high supersaturations and is the signature of the instability of the initial polygonal crystal shape due to local perturbations, notably a nonuniformity in the supersaturation around the growing crystal (Chernov, 1984). The crystal encountering a protein-rich droplet experiences a profound perturbation in the local supersaturation and, most importantly, now has a large amount of protein newly available. Thus, when a crystal grown at pH 7 touches a protein-rich droplet it quickly propagates inside the droplet. In contrast, regardless of the supersaturation, the shape of the other polymorph, grown at pH 6.5, was always polygonal and stable in our experimental conditions. Consequently, the difference in the crystal growth mechanisms of the two polymorphs may be attributed to their stability with respect to local perturbations.

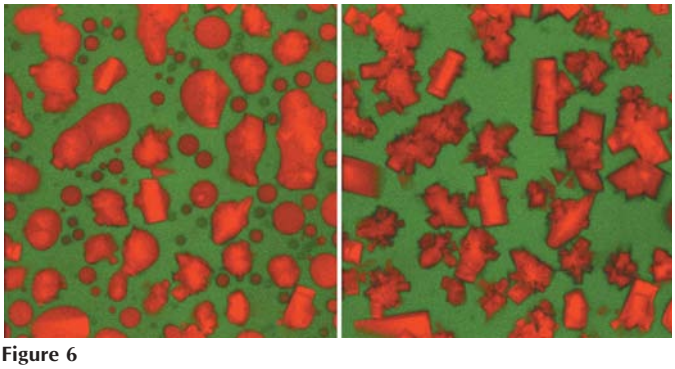

Figure 6
CSLM micrographs of the crystal nucleation and growth mechanism observed at pH 6.5; color convention is as in the lower panels in Fig. 2. The first picture on the left was taken in the first 5 min after mixing and the time interval between the two pictures was 358 s. ($C_{\rm protein} = 75$ mg ml^{-1}, $C_{\rm PEG10\,kDa} = 9\%$, 0.5 *M* NaCl, 10 m*M* MES pH 6.5; dimensions of each picture: 307 × 307 µm).

Quantitative CSLM experiments can also explain the reasons for the contrasting stability patterns, specifically the reason that crystal growth almost ceases as soon as the crystals are no longer in contact with the protein-rich phase. Indeed, outside the dense droplets, the crystal is quickly surrounded by a depletion zone, making the supersaturation at the crystal surface very low. Crystal growth therefore becomes much slower and is probably limited by bulk diffusion. Close to the liquid–liquid phase boundary where the volume of the dense phase is low, the same depletion zone is responsible for crystallization observed partially or totally outside the droplets. Indeed, because of the drop in the protein concentration around the growing crystal, the overall composition drops back below the liquid–liquid boundary and the droplets become unstable and disappear.

6. Conclusions

The *in situ* quantitative measurements using confocal scanning fluorescence microscopy reported here add several novel aspects to the extant knowledge of the coupling of a metastable liquid–liquid phase separation to protein crystallization, in this case for the PEG/glucose isomerase system. Liquid–liquid phase separation produces a very highly concentrated protein solution and a dilute protein solution, with the polymer found mostly in the protein-dilute phase. Crystal nucleation and growth mainly occurred in the protein-rich phase, in agreement with recent theories but at variance with the experimental behavior generally observed previously. The two crystallization mechanisms, producing two different polymorphs, that were characterized illustrate the richness of the problem, specifically the coupling of the features of the equilibrium phase diagram and other physicochemical phenomena, including mass transfer and interfacial properties. With one polymorph, crystal growth occurs 'droplet-by-droplet', while with the other one a 'classical homogeneous' mechanism was observed. In the first case, observation of the droplet-to-droplet behavior depends not just on the concentrations in the respective phases but also on the phase ratio, which determines the local droplet concentration and spacing. The presence of a depletion zone, indicating diffusional limitations, around the growing crystals explains the slower crystal growth once the crystals are no longer in contact with the dense droplet. Such diffusional limitations are also generally implicated in the growth of dendritic crystals, as observed for this polymorph. The presence of a depletion zone is also the reason that crystal growth can take place outside the dense droplets close to the liquid–liquid boundary. The difference in the stability of the two polymorphic crystals with respect to local perturbations could explain the difference between the two mechanisms. Another factor may be the wettability of the crystal

surfaces, which seems to be more highly favored for the second polymorph, allowing those crystals to grow for a more extended period in a high-protein environment. Overall, the multiplicity of phenomena and the sensitivity of behavior to the experimental conditions make this system an excellent one for further exploring the linkage between liquid–liquid phase separation and crystallization.

We are grateful to Dr Kirk Czymmek and J. J. Langford (University of Delaware) for their help during the confocal microscopy experiments, to Dr Kalevi Visuri (Macrocrystal Oy) for useful information about glucose isomerase, and to NASA for financial support under grant number NAG8-1830.

References

Alber, T., Hartman, F. C., Johnson, R. M., Petsko, G. A. & Tsernoglou, D. (1981). *J. Biol. Chem.* **256**, 1356–1361.
Annunziata, O., Asherie, N., Lomakin, A., Pande, J., Ogun, O. & Benedek, G. B. (2002). *Proc. Natl Acad. Sci. USA*, **99**, 14165–14170.
Annunziata, O., Ogun, O. & Benedek, G. B. (2003). *Proc. Natl Acad. Sci. USA*, **100**, 970–974.
Asakura, S. & Oosawa, F. (1958). *J. Polymer Sci.* **33**, 183–192.
Atha, D. H. & Ingham, K. C. (1981). *J. Biol. Chem.* **256**, 12108–12117.
Blonk, J. C. G., van Eendenburg, J., Koning, M. M. G., Weisenborn, P. C. M. & Winkel, C. (1995). *Carbohydr. Polymers*, **28**, 287–295.
Bonnett, P. E., Carpenter, K. J., Dawson, S. & Davey, R. J. (2003). *Chem. Commun.* pp. 698–699.
Budayova, M., Bonneté, F., Tardieu, A. & Vachette, P. (1999). *J. Cryst. Growth*, **196**, 210–219.
Chen, Q., Vekilov, P. G., Nagel, R. L. & Hirsch, R. E. (2004). *Biophys. J.* **86**, 1702–1712.
Chernov, A. A. (1984). *Modern Crystallography III: Crystal Growth.* Berlin/Heidelberg/New York/Tokyo: Springer–Verlag.
Collier, R. J., Westbrook, E. M., McKay, D. B. & Eisenberg, D. (1982). *J. Biol. Chem.* **257**, 5283–5285.
Faers, M. A. & Luckham, P. F. (1997). *Langmuir*, **13**, 2922–2931.
Galkin, O. & Vekilov, P. G. (2000). *Proc. Natl Acad. Sci. USA*, **97**, 6277–6281.
Haas, C. & Drenth, J. (1998). *J. Phys. Chem. B*, **102**, 4226–4232.
Haas, C. & Drenth, J. (2000). *J. Phys. Chem. B*, **104**, 368–377.
Hachisu, S. (1998). *Croat. Chem. Acta*, **71**, 975–981.
Harris, L. J., Skaletsky, E. & McPherson, A. (1995). *Proteins*, **23**, 285–289.
Hoog, E. H. A. de, Kegel, W. K., van Blaaderen, A. & Lekkerkerker, H. N. W. (2001). *Phys. Rev. E*, **64**, 021407.
Kam, Z. & Feher, G. (1978). *J. Mol. Biol.* **123**, 539–555.
Komatsu, H., Miyashita, S. & Suzuki, Y. (1993). *Jpn J. Appl. Phys.* **32**, L1855–L1857.
Kuciel, R., Jakob, C. G., Lebioda, L. & Ostrowski, W. S. (1992). *J. Cryst. Growth*, **122**, 199–203.
Kulkarni, A. & Zukoski, C. F. (2001). *J. Cryst. Growth*, **232**, 156–164.
Kuznetsov, Y. G., Malkin, A. J. & McPherson, A. (2001). *J. Cryst. Growth*, **232**, 30–39.
Michel, H. (1991). Editor. *Crystallization of Membrane Proteins.* Boca Raton: CRC Press.
Muschol, M. & Rosenberger, F. (1997). *J. Chem. Phys.* **107**, 1953–1962.
Nordmark, T. S. & Ziegler, G. R. (2000). *Food Hydrocolloid.* **14**, 579–590.
Ray, W. J. & Bracker, C. E. (1986). *J. Cryst. Growth*, **76**, 562–576.
Schwartz, A. M. & Berglund, K. A. (1999). *J. Cryst. Growth*, **203**, 599–603.
Sukhishvili, S. A., Chen, Y., Muller, J. D., Gratton, E., Schweizer, K. S. & Granick, S. (2002). *Macromolecules*, **35**, 1776–1784.
Tanaka, S. & Ataka, M. (2002). *J. Chem. Phys.* **117**, 3504–3510.
Tanaka, S., Ataka, M., Onuma, K. & Kubota, T. (2003). *Biophys. J.* **84**, 3299–3306.
Tessier, P. M., Johnson, H. R., Pazhianur, R., Berger, B. W., Prentice, J. L., Bahnson, B. J., Sandler, S. I. & Lenhoff, A. M. (2003). *Proteins*, **50**, 303–311.
Vekilov, P. G. (2004). *Cryst. Growth Des.* **4**, 671–685.
Velde, F. van de, Weinbreck, F. Edelman, M. W., van der Linden, E. & Tromp, R. H. (2003). *Colloid. Surf. B*, **31**, 159–168.
Vivarès, D. & Bonneté, F. (2002). *Acta Cryst.* D**58**, 472–479.
Vivarès, D. & Bonneté, F. (2004). *J. Phys. Chem. B*, **108**, 6498–6507.
Vrij, A. (1976). *Pure Appl. Chem.* **48**, 471–483.
Wolde, P. R. ten & Frenkel, D. (1997). *Science*, **277**, 1975–1978.